Investigations on the Peach 4 debrite, a late Pleistocene mass movement on the northwest British continental margin

Matthew Owen[a*], Simon Day[b], David Long[c] and Mark Maslin[a]

a. Environmental Change Research Centre, Department of Geography, University College London, Gower Street, London WC1E 6BT. UK.

b. Aon Benfield UCL Hazard Research Centre , Department of Earth Sciences, University College London, Gower Street, London WC1E 6BT. UK.

c. British Geological Survey, Murchison House, West Mains Road, Edinburgh EH9 3LA. UK.

*. Corresponding author: m.owen@ucl.ac.uk

Abstract

The Peach 4 debrite is the most recent in a series of large scale Pleistocene MTDs within the Barra fan on the northwest British continental margin. Geophysical data indicate that Peach 4 was formed through a combination of blocky and muddy debris flows and affects an area of ~ 700 km^2. BGS core sample 56 -10 36, located directly over the Peach 4 debrite, provides a minimum age of 14.68 ka cal BP for the last major failure. An upwards fining turbidite sequence in BGS core sample 56 -10 239 is associated with increased As and S concentrations, indicators of diagenetic pyrite which forms under anoxic conditions. It is proposed that As and S concentrations may provide a method of distinguishing between contourite and turbidite sedimentation, though further research is required.

Keywords: Submarine mass movement, submarine landslide, mass transport deposit, debrite, debris flow, turbidite, Barra fan, British ice sheet, arsenic, sulphur, pyrite.

1 Regional setting and sedimentation on the Barra fan

The Peach 4 debrite is located on the northwest British continental margin within the Barra fan. Sedimentation on the fan is governed by a combination of down-slope and across-slope mechanisms. The primary across slope process is driven by contouritic current circulation, resulting in contourite deposits such as the Barra Fan Drift. This deposit consists of sediment waves with a length of ~ 3 km and height of 15-30 m, smaller local contourite deposits are also located on the Barra Fan (Knutz et al. 2002).

The largest down-slope sedimentation feature on the Barra Fan is the Peach debris flow complex, the location of which is shown on Figure 1a. Holmes et al. (1998) mapped the complex, which covers an area of ~1600 km^2, identified four major units of Pleistocene age: debrite 1 (823 km^3), debrite 2 (673 km^3), debrite 3 (199 km^3) and debrite 4 (135 km^3). Using the age/depth profile of Knutz et al. (2001), Maslin et al. (2004) estimated the age of the three most recent debrites: 2, 3 and 4 as 36.5, 21 and 10.5 ka cal BP respectively; this most recent date we revise below.

This paper first investigates the morphology and timing of the Peach 4 debrite and then analyses the sedimentology and geochemistry of a sediment core from the boundary of the major failure in order to try and understand the recent sedimentation processes.

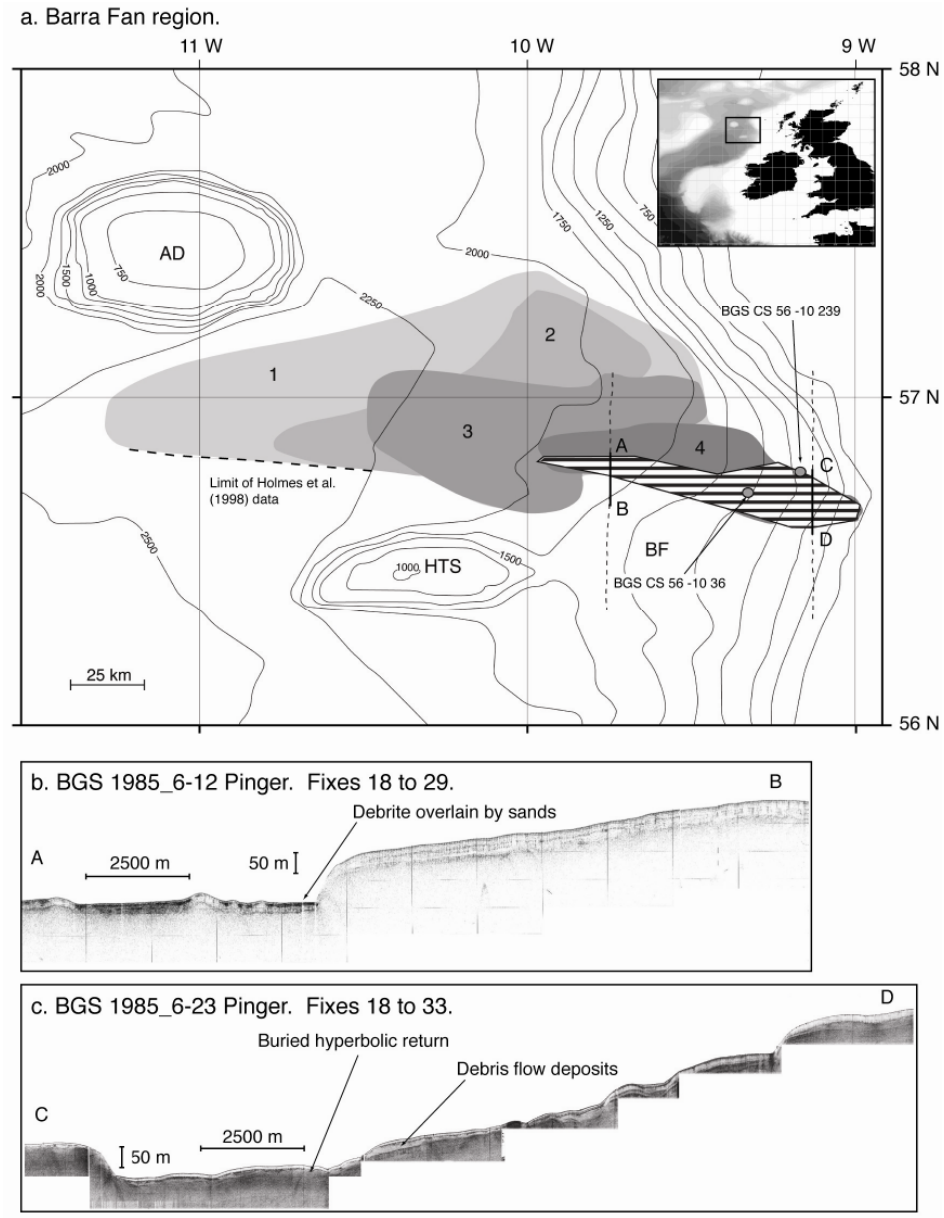

Figure 1: Regional setting of the Peach debris flow complex. a. The Barra fan region with the approximate extents of Peach debrites 1-4 (from Holmes et al. 1998) hatched area indicates zone of major failure, BGS seismic lines 1985_6-12 and 6-23, Barra fan (BF), Anton Dohrn seamount (AD) and Hebrides Terrace seamount (HTS) shown; b and c. 3.5 kHz lines 1985_6-12 and 6-23 plotted with × 10 vertical exaggeration.

2 Methods

2.1 Geophysical data and model construction

This project utilises British Geological Survey 3.5 kHz Pinger and Deep Towed Boomer data, and LOIS Shelf Edge Survey Multibeam Echo sounder (MBE) data. The 3" reso-

lution of the MBE data at this latitude represents 50 m resolution in Easting and 90 m in Northing. All positional data was converted to WGS 84 UTM and then plotted, with sediment core sample positions, in AutoCad: producing a model covering the area between 56.5° N -9.0° W and 57.0° N -10.0° W. Rendering of the DTM was performed with an artificial light source from the north-northeast to allow clearer 2D presentation.

2.2 Sediment samples

BGS CS 56 -10 36 was collected at 1290 mbsl, 56.7095° N -9.3275° W and has been described previously (see Kroon et al. 1997; Kroon et al. 2000). Kroon et al. (2000) date planktonic foraminifera from 4.3 m depth in the core at 12.62 reservoir corrected ^{14}C ka BP, corresponding to 14.68 ka cal BP (Fairbanks et al. 2005).

The sediment analysis presented here focuses on BGS CS 56 -10 239 which was collected at 1030 mbsl, 56.7822° N -9.1698° W. It was sub-sampled at 2 cm intervals for the first 2 m of its length with continuous 2 cm samples taken between 0.92 – 0.98, 1.92 – 1.98 and 2.07 – 2.13 m; between 2.00 – 2.07 and 2.15 and 2.50 m the core was sampled at 1 cm intervals.

2.2.1 Particle size analysis

Sub-samples were freeze-dried and then wet-sieved between 250 and 63 µm (2 - 4 Φ), analysis of < 63 µm diameter fraction was performed by SediGraph 5120 and > 250 µm by dry sieving. SediGraph analysis was performed on a solution concentration of < 3% (see Coakley and Syvitski 1991). Up to 8 analyses were performed on each sub-sample and standard deviations were low compared to inter-sample variability.

2.2.2 XRF geochemical analysis

Prior to wet sieving ~4 g of freeze-dried bulk sediment from each sub-sample was finely ground, weighed and placed in containers with a tightly stretched polypropylene film base. Analysis was performed under Helium gas flush (for further detail regarding XRF methodology under Helium gas flush see Wien et al. 2007). Samples were analysed up to four times and standard deviations were low relative to inter-sample variability.

3 Peach 4 debrite transport processes and age of emplacement

3.1 Extent and morphology of the Peach 4 debite

The primary failure zone of debrite 4 has an area of approximately 700 km^2, failure scarps with heights of up to 90 m are observed and runout distance is at least 60 km. The greatest slope angles were observed on the northern and northeastern debrite boundary (up to 11.8°), associated with a scarp slope of up to 90 m height. The southern boundary of the debrite is associated with gentler angles of around 6.4° and a maximum scarp slope height of 50 - 60 m. The majority of the debrite deposits are overlain by a sedimentary unit between 5 and 11 ms TWT thick. Assuming sound velocity of 1650 m/s^{-1} through these sediments the thickness may be estimated at 4 to 9 m. Outside of this major failure zone a secondary zone of less deep-seated failures is observed. Immediately south from the major scar a smaller slump scar and deposit are visible (Fig. 2c). North from the major failure seismic data reveal surficial sediment failures, which may be associated with the Peach 4 debrite (Fig. 2b).

Several distinct MTD seismic facies are clearly visible (Figs. 1b, c, and 2b). Highly acoustically transparent, mounded facies, with sharp basal contacts, are potentially de-

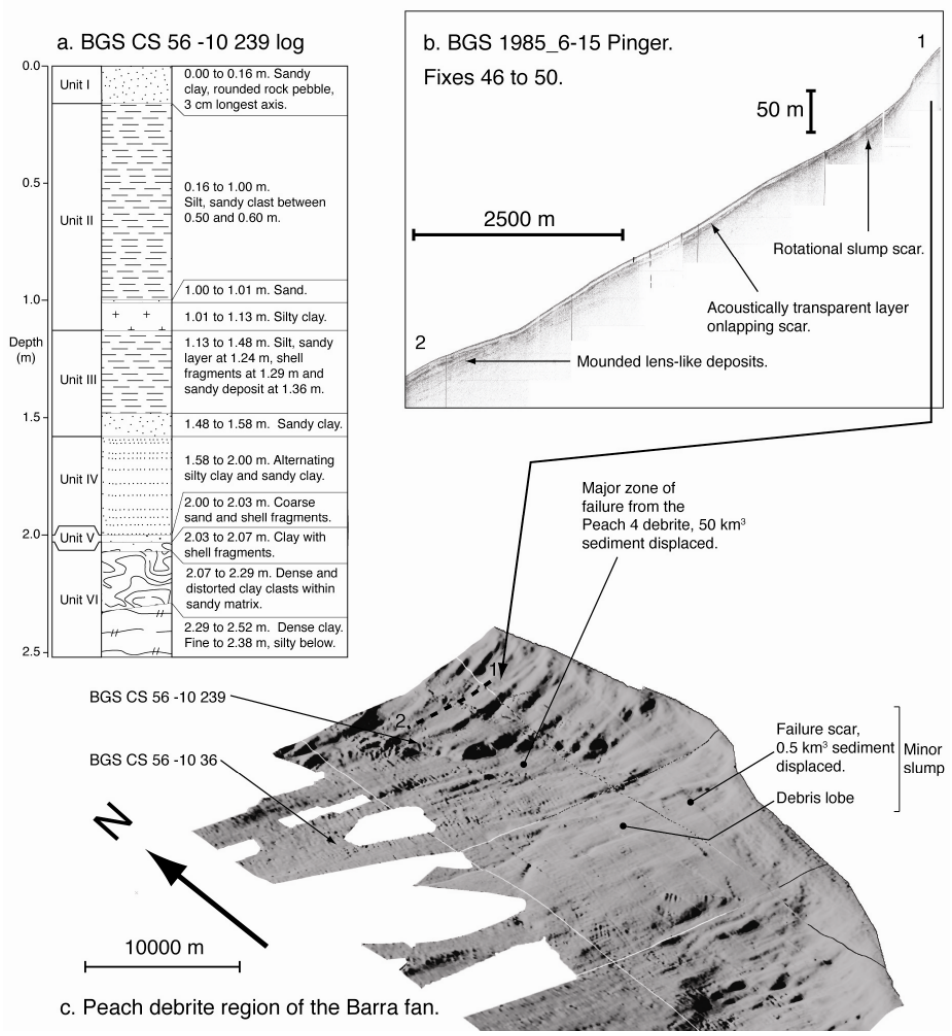

Figure 2: Location and description of gravity core BGS CS 56 -10 239: a. BGS CS 56 -10 239 log; b. BGS 3.5 kHz profile, 1985_6-15, shown with a × 10 vertical exaggeration; and c. Shaded relief shown with a 4 × vertical exaggeration and light from the NNW, locations of BGS CS 56 -10 36 and 56 -10 239 shown.

posited from muddy debris flows (see Embley 1980; Piper et al. 1999). Buried, or surficial, hummocky, blocky facies with hyperbolae are indicative of larger debris (Jacobi 1976; Normark and Gutmacher 1988) . Also visible in Figure 1b are stratified and high amplitude facies which overlie blocky, chaotic facies: these are interpreted as sands (contourite or turbidite) overlying debris flow deposits. Armishaw et al. (1998) state that the Peach debrite is a composite feature. In a similar manner, Peach 4 has been formed through the action of several mass movement mechanisms within one event. The different seismic facies observed, supports a combination of blocky debris flows, muddy debris flows and possibly sandy turbidites contributing to the overall structure of the Peach 4 debrite.

3.3 Emplacement age of the Peach 4 debrite

The model constructed for this project locates BGS CS 56 -10 36 in hemipelagic sediments overlying deposits from the Peach 4 debrite (see Fig. 2c). This means that this

core constrains the minimum age of Peach 4. Combined with Holmes et al. (1998) argument that the Peach 4 debrite truncates ice-berg scour marks, this suggests that the timing can be constrained to between 14.68 (the oldest material within BGS CS 56 -10 36 dated by Kroon et al. 2000) and 19 ka cal BP (the oldest estimate for the disintegration of the BIS in the Barra fan region; Knutz et al. 2007).
Kroon et al. (2000) date the Bölling period, using planktonic foraminiferal assemblages, at slightly after 14.6 ka cal BP in the Barra fan region (Kroon et al. 2000 ^{14}C dates, Fairbanks et al. 2005 radiocarbon calibration). Coupled with the marine data from Knutz (2007) it seems plausible that factors associated with the deglaciation may have played a role in increasing the susceptibility of the continental slope to failure and increasing the likelihood of triggers to slope failure occurring (see Owen et al., 2007).

4 Sediment analysis results and interpretation for BGS CS 56 -10 239

4.1 Location of BGS CS 56 -10 239 in relation to MTDs

BGS CS 56 -10 239 is located on the northeastern boundary of the Peach 4 failure, though within the zone of minor sedimentary failure (see Fig. 2c). Upslope from the core BGS 3.5 kHz Pinger profile 1985_6-15 (Fig. 2b) reveals a rotational, scoop-like, slump scar containing lensed slump deposits. Onlapping and downslope of these, is a unit with a strong seabed return over an acoustically transparent layer (3 ms TWT thick) which in turn overlies chaotic and distorted facies which are likely the disaggregated blocky deposits of the rotational failure. Downslope mounded lens-like deposits are visible as acoustically transparent units with a high amplitude upper boundary.

4.2 Particle size variations

Particle size analysis results are summarised in Figure 3. Mean grain size decreases from 4 to 7 Φ from seabed to 0.16 m depth, this is due to the shift from foraminiferal sand to terrigenous silt and clay dominated sediments. Φ and sand/silt/clay percentages are relatively constant until 1.13 m when there is a peak in clay composition of 54%.
Between 1.13 and 1.55 m depth there is a stepped increase in mean grain size, which is

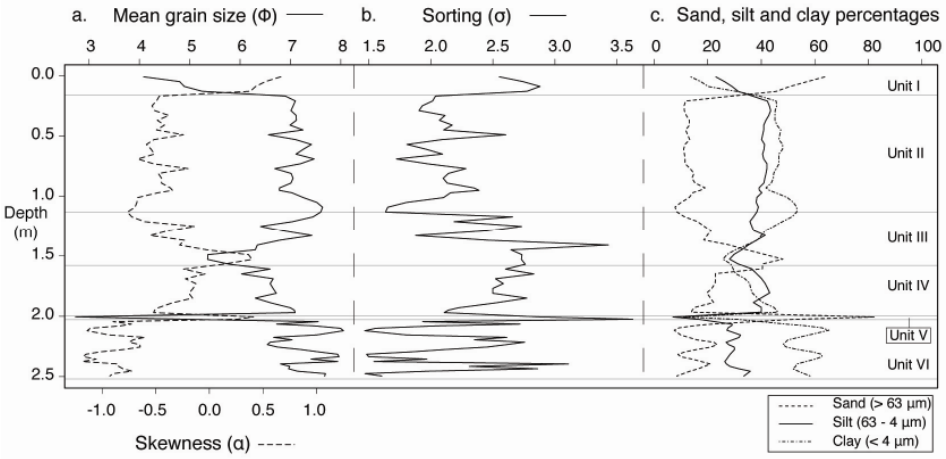

Figure 3: Particle size analysis for BGS CS 56 -10 239. a. Mean grain size and skewness; b. Sorting; and c. Sand, silt and clay percentage composition

coincident with a minor peak in silt composition at 1.25 m and a major sand peak of 48% at 1.55 m. σ also displays a stepped trend during this interval, with a succession of poorly sorted to very poorly sorted sediments between 1.13 and 1.25 m and between 1.33 and 1.41 m. Between 1.55 and 2.00m Φ values increase to 7 reflecting the decrease in the proportion of sand particles and the increase in silts and clays; sediments remain very poorly sorted though silt is the dominant size class. At 2.00 m a large increase in particle size occurs associated with a 3 cm thick erosive sand layer. Below 2.03 m there are two pronounced oscillations in Φ values between 7 and 8, which are reflected in inversely related sand and clay percentages, σ values shifting from poorly sorted to very poorly sorted.

4.3 XRF geochemical analysis

The results for bulk sediment sample data for Ca, Fe, S and As contents are presented in Figure 4. Ca declines sharply, from > 12.0% to levels ~ 6.0% below 0.16 m. An increase to 8.0% at 1.53 m is coincident the 48% sand peak at 1.55 m (see Fig. 3). Other than the initial increase in concentrations (1.8 - 3.9 %) the primary feature of note in the Fe record is a marked reduction in concentrations (4.0 - 2.8 %) between 1.13 and 2.03 m, coincident with the increase in sand (and decrease in clay) content, as shown in Figure 3. With the exception of an isolated peak at 0.81 m, S concentrations are close to 0.0% between 0.0 and 1.00 m. However, a dramatic increase occurs from 1.13 m as values peak at 0.27% concentration at 1.37 m depth. S concentrations then decline to ~ 0.15% before peaking again at 0.26% at 1.65 m, prior to declining to background levels below 2.00 m. Elevated S levels are bracketed by a primary As peak of 40 µg/g at 1.21 m and a secondary As peak of 31 µg/g at 2.12 m.

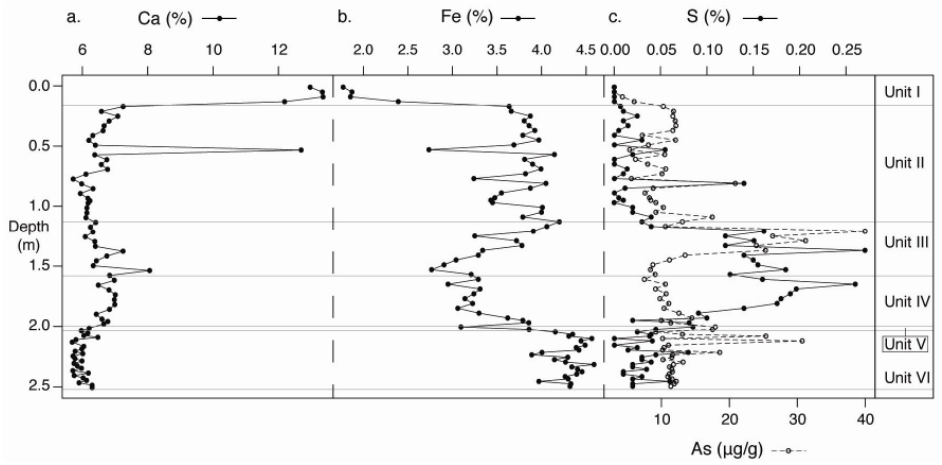

Figure 4: Selected XRF analysis result for BGS CS 56 -10 239. a. Calcium; b. Iron; and c. Sulphur (all plotted as percentage bulk sediment) and Arsenic (µg/g bulk sediment).

4.4 Unit Lithology of BGS 56 -10 239

BGS CS 56 -10 239 is subdivided into six lithological units on the basis of the visual inspection and particle size analysis:

1. Unit I: sandy sediments with high Ca and low Fe content indicating a dominant marine sediment source (0.0 to 0.16 m), likely to be Holocene drape or contourites.
2. Unit II: mainly silts and clays with low Ca and high Fe content indicating a dominant

terrestrial sediment source (0.16 to 1.13 m). The unit displays a sharp upper boundary, whereas the lower boundary is less distinct, probably due to bioturbation. Likely to be hemipelagite.

3. Unit III: clays, silts and sand layers with frequent shell fragments (1.13 to 1.58 m), interpreted as a succession of turbidites. Particle size data (Fig. 3) supports this interpretation with a stepped upwards fining and alternation between less sorted (associated with coarser grains) and more sorted (associated with finer grains) sediments. This unit has a distinct geochemical signature, with Fe concentrations reducing down core, a pronounced As peak and elevated S concentrations (see Fig. 4).
4. Unit IV: alternating sandy clay and silty clay, in which silts are the dominant fraction (1.58 to 2.00 m), possibly hemipelagic or contouritic sediments. Fe concentrations remain low, S concentrations relatively high and, distinct from unit III, As concentrations return to background levels (see Fig. 4).
5. Unit V: a coarse grained, poorly sorted, sand layer with large shell fragments (2.00 to 2.03 m), which erodes into the unit below and is interpreted as a turbidite.
6. Unit VI: dense and distorted clay intraclasts with sandy matrices (2.03 to 2.52 m). From 2.03 to 2.29 m the unit is characterised by highly distorted clay clasts, at times within a sandy matrix. Below 2.29 m the appearance is more homogeneous. Oscillating mean grain size and sorting values (see Fig. 3), supports a debris flow hypothesis for the formation of this unit; potentially through as succession of slurries or as a low-viscosity cohesive debris flow (see Tripsanas et al. 2008).

We can therefore be certain that units V and VI are associated with mass transport, and units I and II with background sedimenation (pelagic, hemipelagic or contouritic) which postdates mass transport. Difficulty occurs when attempting to assign units III and IV to either mass transport or background sedimentation. This ambiguity has important implications when attempting to date mass transported material through use of overlying sediments. We now consider whether geochemical data can help resolve this issue.

5 Sedimentation processes in BGS CS 56 -10 239 - Can sulphur and arsenic concentrations be used as indicators of turbidite deposition?

The difficulty of distinguishing between sandy turbidites and sandy contourites in marine sediments is well known (Stow 1979) and it is well established that these are important components of the Barra fan sedimentary system (see Armishaw et al. 2000; Knutz et al. 2002). We consider whether S and As concentrations can be used to distinguish between turbidites and contourites.

A striking feature of unit III is a marked increase in As and S concentrations, inversely related to Fe (see Fig. 4). We hypothesise that this is due to the rapid deposition of sediments which create anoxic conditions, favourable to pyrite (FeS_2) formation through organic matter decomposition via the actions of sulphate reducing bacteria (see Berner and Raiswell 1983). The As peak at 1.21 m (potentially a signal from arsenian pyrite) provides further support for this hypothesis, as As in marine sediments is generally an indicator of FeS_2 (Rothwell et al. 2006), which has been shown to be enriched in As by as much as 10% wt (Blanchard et al. 2007). The peak in clay particle composition, directly above the As peak, at 1.13 m further supports this hypothesis as formation of As enriched FeS_2 generally occurs in colloidal sized particles (Cook and Chryssoulis 1990). The organic matter required for FeS_2 formation in the the anoxic environment created by

the rapid deposition of unit III is possibly provided by unit IV. This unit is characterised by an upwards coarsening of sediments and high concentrations of silt particles (Fig. 3a), possibly indicating a strengthening of contouritic currents. High concentrations of S are maintained, though As concentrations return to background levels.
It is possible that the As and S record is displaying two separate signatures: increased S concentrations related to increased organic matter concentrations (Berner and Raiswell 1983), primarily in unit IV; and increased As and S concentrations due to production of diagenetic pyrite (Blanchard et al. 2007) under anoxic conditions in the interstital waters of unit III. Increased As and S concentrations may then be a potential indicator of anoxic conditions caused through rapid sedimenation; and combined elevated concentrations of both elements may be indicate turbidite rather than contourite sedimentation.
Alternatively, anoxia and FeS_2 formation may have occurred via through flow of geologically derived CH_4 through the more permeable sandy layers. Further research is required: sedimentation in the region is extremely complex with both contourite and turbidite sediments potentially being reworked. As such a unit may display the sedimentological characteristics of a contourite and the geochemical signature of a turbidite. Investigations into benthic foraminiferal assemblages and TOC content would provide insights into whether sediments have been subject to mass transport and whether S concentrations are reflecting a diagenetic or primary signal.

6 Conclusions

1. The most recent MTD in the Peach slide complex was deposited through a combination of blocky debris flows and low viscosity cohesive debris flows. The primary zone of failure has an area of approximately 700 km^2.
2. The positioning of BGS CS 56 -10 36 helps constrain the timing of the Peach 4 debrite's major failure to between 14.68 and 19 ka cal BP.
3. A turbidite succession in BGS CS 56 -10 239 is associated with a substantial increase in As and S concentrations. It is proposed that rapid deposition of sands, capped with silts and clays, creates anoxic conditions favourable to the formation of diagenetic pyrite. We suggest that elevated As and S concentrations within sediments may provide a means of distinguishing turbidite from contourite sediments.
4. Further work is required: analysis of benthic foraminiferal assemblages and TOC content will provide greater insight into whether sediments have been subject to mass transport and what processes are controlling S and As concentrations.

7 References

Armishaw JE, Holmes RW, Stow DAV (2000) The Barra Fan: A bottom-current reworked, glacially-fed submarine fan system. Mar Pet Geol 17:219–238.

Berner RA, Raiswell R (1983) Burial of organic carbon and pyrite sulfur in sediments over Phanerozoic time: a new theory. Geochim Cosmochim Ac 47:855-862.

Blanchard M, Alfredsson M, Brodholt J et al (2007) Arsenic incorporation into FeS_2 pyrite and its influence on dissolution: A DFT study. Geochim Cosmochim Ac 71:624-630.

Coakley JP, Syvitski JPM (1991) SediGraph technique. In Syvitski JPM (ed), Principles, methods and applications of particle size analysis. Cambridge University Press.

Cook NJ, Chryssoulis, SL (1990), 'Concentrations of invisible gold in the common sulfides', Can Mineral 28:1-16.

Embley RW (1980) The role of mass transport in the distribution of deep-ocean sediments with special reference to the north atlantic. Mar Geol 38:23-50.

Fairbanks R, Mortlock R, Chiu T et al (2005) Radiocarbon calibration curve spanning 0 to 50,000 years BP based on paired Th/U/U and C dates on pristine corals. Quaternary Sci Rev 24:1781-1796.

Holmes R, Long D, Dodd LR (1998) Large-scale debrites and submarine landslides on the Barra Fan west of Britain. In: Stoker MS, Evans D, Cramp A (eds) Geological Processes on the Continental margins: Sedimentation, Mass-wasting and stability. Geological Society, London.

Jacobi RD (1976) Sediment slides on the northwestern continental margin of Africa. Mar Geol 22:157-173.

Knutz PC, Austin WEN, Jones EJW (2001) Millenial-scale depositional cycles related to the British ice sheet variability and North Atlantic paleocirculation since 45 kyr B.P., Barra Fan, U.K. margin. Paleoceanography 16:53–64.

Knutz PC, Jones EJW, Austin WEN, et al (2002) Glacimarine slope sedimentation, contourite drifts and bottom current pathways on the Barra Fan, UK North Atlantic Margin. Mar Geol 188:129–146.

Knutz PC, Zahn R, Hall I (2007) Centennial-scale variability of the British Ice Sheet: Implications for climate forcing and Atlantic meridional overturning circulation during the last deglaciation. Paleoceanography. doi:10.1029/2006PA001298.

Kroon D, Austin WEN, Chapman MR et al (1997) Deglacial surface circulation changes in the northeastern Atlantic: Temperature and salinity records of NW Scotland on a century scale. Paleoceanography 12:755-763.

Kroon D, Shimmield G, Austin WEN et al (2000) Century- to millennial-scale sedimentological-geochemical records of glacial-Holocene sediment variations from the Barra Fan (NE Atlantic)', J Geol Soc London 157:643–653.

Maslin M, Owen M, Day S et al (2004). Linking continental-slope failures and climate change: Testing the clathrate gun hypothesis. Geology 32:53–56.

Normark WR, Gutmacher CE (1988) Sur submarine slide, Monterey Fan, central California. Sedimentology 35:629-647.

Owen M, Day S, Maslin M (2007) Late Pleistocene mass movements: occurrence and cause. Quaternary Sci Rev 26:958-978

Piper DJW, Hiscott RN, Normark WR (1999) Outcrop-scale acoustic facies analysis and latest Quaternary development of Hueneme and Dume submarine fans, offshore California. Sedimentology 46: 47-78.

Rothwell GR, Hoogakker B, Thomson J et al (2006) Turbidite emplacement on the southern Balearic Abyssal Plain (western Mediterranean Sea) during Marine Isotope Stages 1-3: an application of ITRAX XRF scanning of sediment cores to lithostratigraphic analysis. In Rothwell GR (ed) New Techniques in Sediment Core Analysis. Geological Society, London.

Stow DAV (1979) Distinguishing between fine-grained turbidites and contourites on the Nova Scotian deep water margin. Sedimentology 26:371-387.

Tripsanas E, Piper D, Jenner K et al (2008) Submarine mass-transport facies: new perspectives on flow processes from cores on the eastern North American margin. Sedimentology 55:97-136.

Wien K, Kölling M, Schulz HD (2007) Age models for the Cape Blanc Debris Flow and the Mauritania Slide Complex in the Atlantic Ocean off NW Africa. Quaternary Sci Rev 26:2558-2573.

Acknowledgments

The authors thank: the reviewers R Wynn and E Tripsanas for their constructive comments; G Tulloch, J Hope, T Maxted and I Patmore for assistance with sediment analysis. MO thanks the UCL Graduate School, the ECRC and ENSIS trust fund. DL publishes with permission of the Executive Director, British Geological Survey (NERC).